A systematic assessment of structural heterogeneity and IgG/IgE-binding of ovalbumin

Wenhua Yang,[1, 2, 4, ✉] Zongcai Tu,[2, 3, ✉] David Julian McClements[5] and Igor A. Kaltashov[4]

[1] College of Chemistry and Bioengineering, Yichun University, Yichun, Jiangxi, 336000, People's Republic of China

[2] State Key Laboratory of Food Science and Technology, Nanchang University, Nanchang, Jiangxi, 330047, People's Republic of China

[3] National R&D Center of Freshwater Fish Processing, and Engineering Research Center of Freshwater Fish High-value Utilization of Jiangxi Province, Jiangxi Normal University, Nanchang, 330022, People's Republic of China

[4] Department of Chemistry, University of Massachusetts-Amherst, Amherst, MA, 01003, USA

[5] Department of Food Science, University of Massachusetts-Amherst, Amherst, MA, 01003, USA

✉ address correspondence to: ***Wenhua Yang***, College of Chemistry and Bioengineering, Yichun University, Yichun, Jiangxi, PRC, 336000, email: yangwh88@hotmail.com and ***Zongcai Tu***, State Key Laboratory of Food Science and Technology, Nanchang University, 235 Nanjingdonglu, SKLF 108, Nanchang, Jiangxi, PRC, 330047, email: tuzc_mail@aliyun.com

Abstract

Ovalbumin (OVA), one of the major allergens in hen egg, exhibits extensive structural heterogeneity due to a range of post-translational modifications (PTMs). However, analyzing the structural heterogeneity of native OVA is challenging, and the relationship between heterogeneity and IgG/IgE-binding of OVA remains unclear. In this work, ion exchange chromatography (IXC) with salt gradient elution and on-line detection by native electrospray ionization mass spectrometry (ESI MS) was used to assess the structural heterogeneity of OVA, while inhibition-ELISA was used to assess the IgG/IgE binding characteristics of OVA. Over 130 different OVA proteoforms (including glycan-free species and 32 pairs of isobaric species) were identified. Proteoforms with acetylation, phosphorylation, oxidation and succinimide modifications had reduced IgG/IgE binding capacities, whereas those with few structural modifications had higher IgG/IgE binding capacities. OVA isoforms with a sialic acid-containing glycan modification had the highest IgG/IgE binding capacity. Our results demonstrate that on-line native IXC/MS with salt gradient elution can be used for rapid assessment of the structural heterogeneity of proteins. An improved understanding of the relationship between IgG/IgE binding capacity and OVA structure provides a basis for developing biotechnology or food processing methods for reducing protein allergenicity reduction.

Keywords: ovalbumin; heterogeneity; ion exchange chromatography-mass spectrometry; post-translational modifications; IgG and IgE binding capacities; glycosylation

1. Introduction

Ovalbumin (OVA), which accounts for about 54% of the protein mass of chicken egg white, is widely used in the food industry due to its excellent nutritional value and functional attributes.[1] However, it is also known to be one of the main allergens in the human diet, which has been linked to up to 8% of all food allergies in infants and young children.[2] Despite being relatively modest in size, consisting of a single polypeptide chain with 385 amino acid residues and a molecular weight of approximately 45 kDa, this glycoprotein is known to be subject to numerous post-translational modifications (PTMs). In addition to the extensive glycosylation (N292), these include N-terminal acetylation (G1), and phosphorylation (at S68 and S344).[3] While both glycosylation and phosphorylation are known to play an important role in protein allergenicity,[4-6] it remains to be seen if other PTMs commonly occurring in OVA may endow this protein with pro- or anti-allergenic properties. However, there have been few systematic studies on the structural heterogeneity caused by PTMs of native OVA molecules. As a result, the relationship between structural heterogeneity and IgG/IgE binding of OVA is currently unclear.

A recent mass spectrometry analysis of OVA revealed the presence of 59 protein isoforms in a commercial sample,[7] which vastly outnumbers the reported number of isoforms that have been detected using separation techniques.[8] However, mass spectrometry has three important limitations. First, it cannot readily make distinctions among isomers, *e.g*. OVA phosphorylation at either of the two possible sites gives rise to two different species with identical masses. Second, simultaneous detection of a large number of protein isoforms raises concerns about the dynamic range of the measurements, such as the "competition for charges" among various protein species and “spectral crowding” leading to a loss of the signal of low-abundance species on the background of highly abundant ones with close *m/z* values. Third, analysis of a glycosylated and/or phosphorylated protein, such as OVA, relies on enzymatic pre-treatment as a means of reducing sample complexity. In addition to increasing the analysis time, these steps may lead to the loss of low-abundance species and introduction of artifacts (non-

enzymatic PTMs that were not originally present in the protein sample).[9, 10]

These challenges can be addressed by combining MS profiling of the protein isoforms with on-line separation technologies. Ion-exchange liquid chromatography (IXC)[11] is particularly useful in this regard, as many common PTMs change either the p*I* or the surface charge distribution patterns within a protein, thus providing a physicochemical basis for separations based on electrostatic interactions. The ability to separate various OVA proteoforms (especially those that differ from each other by net charge) would be beneficial for detecting low-abundance species by spreading the detection over time and avoiding both signal suppression and signal interference within the mass spectrometer. Furthermore, the ability of IXC to separate isomeric species with identical net charges but different local charge patterns[12] should allow a distinction to be made among isobaric species, *e.g.*, the two mono-phosphorylated forms of the protein, as discussed earlier. Since both IXC and MS can be operated under non-denaturing conditions, the on-line IXC/MS measurements (in contrast to the commonly used reversed-phase LC/MS) also allows the conformational integrity of each protein isoform to be assessed based on the ionic charge state distributions in mass spectra.[13] Lastly, native MS frequently provides an advantage for separating the ionic signals of proteins whose masses differ significantly. Indeed, it is known that the extent of multiple charging of protein ions in the gas phase is determined by their physical dimensions in solution.[14, 15] Consequently, ionic signals of two (or more) proteins with vastly different physical dimensions will populate distinct *m/z* regions in the native ESI mass spectrum, thereby reducing the likelihood of or indeed eliminating the signal interference.

Native IXC/MS has been used to characterize therapeutic proteins with extensive PTMs[12, 16-19] and protein-drug conjugates;[20] however, the total number of detected/identified protein isoforms remained relatively modest (not exceeding a couple of dozen in each case). More recently, IXC/MS with pH gradient elution was employed for the characterization of commercial OVA, in which 151 different proteoforms were detected.[21] However, nearly one-third of all these detected isoforms were protein dimers and truncated polypeptide chains,

suggesting that the sub-optimal protocols for manufacturing and handling commercial samples are likely to result in artifacts that may hide/obscure the presence of relevant PTMs. Furthermore, OVA with different PTMs might exhibit variations in their IgG and IgE binding capacities. However, there are few studies on the relationship between structural heterogeneity and IgG/IgE binding of OVA. The objective of this work was therefore to systematically analyze the heterogeneity of native OVA and explore the relationship between OVA heterogeneity and its IgG/IgE binding capacities. To this end, native IXC/MS was used as a means of profiling PTMs within a monomeric OVA sample extracted from hen egg and purified by size-exclusion chromatography (SEC). The IgG/IgE binding of OVA proteoforms were evaluated using an inhibition enzyme-linked immunosorbent assay (ELISA). The results obtained indicate that native IXC/MS was ideally suited for rapid characterization of OVA heterogeneity caused by PTMs and that there is a correlation between structural heterogeneity and variation in IgG/IgE binding of OVA. The methodology presented in this work could provide a basis for controlling the allergenicity of OVA, as well as other allergenic proteins encountered in food, by biotechnology or food processing methods targeting specific PTMs.

2. Materials and methods

2.1 Materials

Goat anti-human IgE-HRP conjugate (A9667), goat anti-rabbit IgG-HRP conjugate (AP187P), commercial standard OVA (A5503) tween-20 and 3,3',5,5'-tetramethylbenzidine (TMB) and were purchased from Sigma-Aldrich (St. Louis, MO, USA). Hen egg allergy (HEA) patients' antisera were obtained from PlasmaLab International (Everett, W.A., USA) and their specific IgE levels ranged from 10.8 kU L^{-1} to 64.6 kU L^{-1} (detailed information is shown in ***Table S1*** in ***Supplementary Information***). The polyclonal anti-OVA sera were produced by male Japanese rabbits (three months old, about 2.0 kg) [Permission No. SCXK(Gan)-2014-0005].[22] All other chemicals and solvents used were of analytical grade or higher.

2.2 Sample preparation

OVA was extracted from chicken egg white using a procedure described in detail elsewhere[1] with some modifications. Briefly, egg white was separated from hen egg and diluted in deionized water. Then its pH was adjusted to 5.5, followed by centrifugation at 3000 g for 20 min at 4 ºC. Ammonium sulfate was added to the supernatant to 50% saturation, followed by pH adjustment to 4.5 and repeated centrifugation. The precipitate was re-dissolved in 0.1 mM EDTA, followed by addition of ammonium sulfate to 38% saturation and centrifugation; this step was repeated twice, yielding crude OVA (the precipitate). After dissolution in deionized water, crude OVA was dialyzed at room temperature under running water for 24 h, and then lyophilized. The lyophilized protein was re-dissolved in 50 mM ammonium acetate and fractionated by SEC using a TSKgel G3000SW$_{XL}$ (Tosoh Bioscience LLC, King of Prussia, PA) column on an HP1100 (Agilent Technologies, Santa Clara, CA) liquid chromatograph at a flow rate of 0.75 mL min^{-1}. The monomeric OVA fraction was collected, lyophilized and re-run on SEC to ensure sample stability. No additional chemical/enzymatic treatment of the protein sample was carried out prior to native IXC/MS analysis. A protein stock solution was prepared by dissolving SEC-purified and lyophilized OVA in 50 mM ammonium acetate and stored at 4 °C.

2.3 On-line IXC/MS

Separations were carried out using a ProPac SAX-10 column (Thermo Fisher Scientific, Waltham, MA) on an HP1100 liquid chromatograph (Agilent Technologies, Santa Clara, CA). Ammonium acetate was used as a mobile phase (50 mM in mobile phase A and 500 mM in mobile phase B, pH 6.9). A linear gradient (0 to 70 % A over 35 min) at a flow rate of 0.2 mL min^{-1} was used in this work to achieve optimal separation. In a single measurement, a 100 μL aliquot of the analyte solution (2 mg mL^{-1} or ~45 μM) was injected onto the column. The eluate was directed to the ESI source of the mass spectrometer following a 1:7 post-column flow splitting (to achieve the final flow rate of 25 μL min^{-1}). On-line MS detection was carried out with a SolariX 7 (Bruker Daltonics, Billerica, MA) Fourier transform ion cyclotron resonance

(FT ICR) mass spectrometer equipped with a 7 T superconducting magnet and a standard ESI source. ESI-generated ions were accumulated externally prior to injection into the ICR cell. The ion optics parameters were selected to optimize the OVA signal: collision voltage, -14 V; RF frequency, 1.4 MHz; collision RF amplitude; 1300 V_{p-p}. All spectra were recorded using 150 msec-long transients, which allowed 400 mass spectra to be acquired over a one-minute window. Each mass spectrum shown in this work is an average of 5 individual spectra. All data were processed using Bruker BioTools software package. The mass spectral data were analyzed according to the method of Heck[7] using 42,747.68 Da as an average mass of intact (PTM-free) OVA with a single disulfide bond.

2.4 IgG and IgE binding capacities evaluation

IgG and IgE binding of OVA were measured by inhibition ELISA with rabbit antisera and HEA patients' antisera, respectively[23]. First, a 96-well microplate was coated with standard OVA (100 μL per well, 2 μg mL^{-1}) overnight at 4 °C. Then it was blocked with 50 mg mL^{-1} fat-free milk. Subsequently, 50 μL of either pooled rabbit antisera (diluted to1:12800) or pooled HEA patients' antisera (diluted to 1:8) and IXC collected OVA samples (inhibitors) with different concentration (0.5, 1.5, 5, 15, 30, 60 μg mL^{-1}) were added and incubated at 37 °C for 30 min. Then, 100 μL of goat anti-rabbit IgG-HRP conjugate or goat anti-human IgE-HRP conjugate (diluted to 1:5000) was added and incubated at 37 °C for 30 min. Next, the sample was colored by adding 100 μL of TMB solution and incubating for at 37 °C 15 min. Finally, the reaction was stopped by adding 50 μL of 2 M sulfuric acid, and the absorbance was measured at 450 nm using a microplate reader (HF2000, Huaan Magnech, Beijing, China). Every step above included the washing with PBST (0.05% Tween-20 in 50 mM PBS, pH 7.4) for five times. The inhibition rate was calculated as follows: Inhibition = $(1 - B / B_0) \times 100\%$, where B and B_0 are the absorbance values of the well with and without the inhibitor, respectively.[23] IC_{50} is the concentration of inhibitors that causes a 50% inhibition of antibody binding (μg mL^{-1}).

2.5 Statistical Analysis

All experiments were carried out in triplicate and the results are presented as mean value ±

standard deviation (SD). The MS data analysis was carried out using Brucker DataAnalysis 4.4 (Bruker, Billerica, MA) and it was shown using Origin-2017 (OriginLab Corp., Northampton, MA).

3. Results and discussion

3.1 Systematic assessment of OVA structural heterogeneity

Initially, the structural heterogeneity of OVA isolated from hen egg was determined using a combination of size chromatography and mass spectrometry. The final step of OVA extraction from the egg white was purification by SEC, which is commonly used in protein analysis to ensure the absence of both high-molecular weight (aggregates) and low-molecular weight components (degradation products resulting from polypeptide chain scission, which are frequently present in commercial products[21]). As shown in **Figure 1**, there were two main peaks in the size exclusion chromatograms. Based on its retention time, the first peak was assigned to ovotransferrin, which is a glycoprotein with a molar mass of about 76 kDa and an isoelectric point of around pH 5.6 to 6.2.[24] After separation, a re-run of the SEC fraction corresponding to OVA monomer yields a well-defined single peak, free of high- or low-molecular weight degradation products (**Figure 1**). A native ESI mass spectrum of this SEC fraction acquired off-line shows an abundant ionic signal confined to an *m/z* region (2800-3800 *u*). The low average charge of the protein ions, and the narrow distribution of the ionic charge states (only charge states +XX through +ZZ are visible in the mass spectrum) are usually interpreted as signs of the protein molecules existing in a compact (natively folded) conformation in solution prior to their transfer to the gas phase.{Itashov, 2008 #2238}[25] Each charge state is represented by a cluster of peaks corresponding to proteins with different masses. Assignment of all of these peaks (highlighted in ***Table S2*** in the ***Supplementary Information***) was facilitated by the availability of an extensive body of knowledge of the PTMs commonly encountered in OVA and thoroughly documented in previous studies.[3, 7, 21, 26] Each of these modifications results in a unique increase of the protein mass (N-terminal acetylation, +42.0

193 Da; phosphorylation, +80.0 Da; succinimide formation, -17.0 Da; oxidation, +16.0 Da;
194 addition of a hexose residue, +162.1 Da; addition of an N-acetyl-hexose amine residue, +203.2
195 Da; addition of an N-acetylneuraminic acid residue, +291.3 Da), although multiple
196 combinations of these modifications may give rise to isobaric species. In addition, the most
197 common PTM expected to occur in OVA is deamidation, but the concomitant mass change
198 associated with this process (1.0 Da) was too small to be measured confidently for this protein.
199 Other common PTMs are N-terminal acetylation, phosphorylation, succinimide formation,
200 oxidation, and glycosylation with hexose, N-acetyl-hexose amine and N-acetylneuraminic acid
201 residues. These OVA isoforms can usually be distinguished from one another based on their
202 masses. Each isoform is represented by a numerical set with each position, indicating the
203 number of structural modifications of a particular kind occurring within the protein (using the
204 same order as listed above). For example, the most abundant OVA proteoform observed in the
205 mass spectrum shown in **Figure 1** can be represented as (1-2-0-0-6-2-0) using this notation,
206 which corresponds to the acetylated, bis-phosphorylated glycoform $Hex_6GlcNAc_2NeuAc_0$
207 lacking structural modifications caused by oxidation and succinimide formation (no
208 assignments can be made about possible deamidation, as discussed earlier).

209 In addition to the high-abundance ionic signal, also visible in the spectrum are low-
210 abundance clusters of ionic peaks, which represent an additional set of OVA proteoforms (also
211 highlighted in ***Table S2*** in the ***Supplementary Information***). Overall, twenty-one proteoforms
212 were detected in the off-line ESI MS analysis of the SEC-purified OVA. This number is
213 significantly below that reported for MS analysis of OVA proteoforms,[7] as no enzymatic pre-
214 treatment of the protein was used in our work. Notably, even though the results of the off-line
215 analysis of the SEC-purified OVA by native ESI MS are consistent with the notion of the
216 protein sample being apparently impurity-free, a magnified view of the ionic signal in the *m/z*
217 region 2200-2900 reveals the presence of several low-abundance ionic species (see the inset in
218 **Figure 1**). It is not clear, however, if these ions represent partially unfolded OVA species (which
219 would be expected to display a higher extent of multiple charging in ESI MS) or other proteins,

as the low intensity of the ionic signal and the extreme crowding of this segment of the mass spectrum made it impossible to extract meaningful information.

Out of the twenty-one major proteoforms detected by MS alone (**Figure 1**), twelve are isobaric species (highlighted red in **Table S1**) that are expected to have different retention characteristics on anion exchange resin. It is not therefore surprising that in stark contrast to SEC, the IXC chromatogram of the OVA sample had a very convoluted shape, with the UV absorption signal spanning over 15 minutes with salt concentrations ranging from 180 mM to 290 mM (the blue trace in **Figure 2A**). On-line detection with native ESI MS generates a chromatogram that generally mirrors the conventional UV absorption signal, but lags slightly behind due to the extra time required for the eluate to reach the ESI source. While the significant time dispersion of OVA species in IXC was not surprising, this protein appears to be only a relatively minor component of the eluate at shorter retention times (< 19 min). Indeed, even though several OVA isoforms can be confidently identified in the first chromatographic peak (a mass spectrum averaged across the 17-18 min elution window is shown in **Figure 2B**), the major protein species have appreciably lower masses. The appearance of the ionic signal at lower *m/z* values (below 3500 *u*) indicates the presence of a heavily glycosylated (and, therefore, highly heterogeneous) protein. Individual ion peaks in each charge state cluster are spaced by 162 and 203 Da, corresponding to the masses of hexose and GlcNAc residues, respectively (indicated by brown and purple arrows in **Figure 2B**). The masses of different glycoforms range from 26.8 kDa to 29.0 kDa, consistent with those of ovomucoid (OVM), one of the most abundant proteins in chicken eggs (accounting, together with OVA and ovotransferrin for nearly 75% of the egg white protein mass).[27] Since the focus of this work was on characterizing the structural micro-heterogeneity of OVA, OVM (eighty-four isoforms found in the OVA sample, as summarized in ***Table S3*** in ***Supplementary Information***) was treated as an impurity and no detailed characterization of its proteoforms was attempted.

Both enzymatic and non-enzymatic PTMs of OVA have been extensively studied in the past, [3, 7, 21, 28, 29] allowing us to make assignments of OVA proteoforms detected by IXC/MS

based on the measured masses. Although native ESI MS has been regarded until recently as a relatively low resolution/accuracy tool for measuring protein masses (mostly due to the extensive adduct formation that results in significant peak broadening and apparent mass shift[30-33]), this problem can be dealt with using efficient thermal desolvation. We have recently demonstrated that mass differences as low as 0.4% can be confidently resolved for protein/ligand complexes as large as 80 kDa in native ESI MS.[34] Other groups have also demonstrated the ability of native ESI MS to provide accuracy in mass measurements that were previously thought to be unattainable using this approach.[7, 35, 36] Among several OVA proteoforms identified within the first IXC chromatographic peak (elution time 17 min), the mass of the most abundant ion corresponds to a glycoform $Hex_9GlcNAc_8NeuAc_0$ incorporating no other PTMs besides acetylation, i.e. isoform (1-0-0-0-9-8-0) using the notations introduced earlier (**Figure 2B**). Interestingly, the extracted ion chromatogram (XIC) of this ionic species plotted across the entire chromatographic run (**Figure 3**) contains an additional peak at 24 min (labeled F in **Figure 3**), which seems puzzling as it is not clear what isobaric forms of this particular species can display such a disparity with regards to their retention behavior on the anion exchange resin. Since OVA has two phosphorylation sites, we also plotted XICs for two ionic species having the same charge state, but higher mass (by 80 kDa and 160 Da, corresponding to the mono- and bis-phosphorylated versions of this glycoform). These XICs are also shown in **Figure 3**. The XIC for the mono-phosphorylated species contains two peaks with elution times of 19.5 (peak B) and 22.5 (peak B) min, while the single peak exhibited by the XIC for the phosphorylated species (peak D) has an elution time of 24.0 min. The elution order of peaks A-D is consistent with the expected retention behavior of different phosphorylation forms of the same protein species, where consecutive addition of anionic groups leads to longer retention. The appearance of two peaks in XIC of the mono-phosphorylated form (peaks B and C) is not surprising, as the retention characteristics on ion exchange resins are known to be attenuated by distribution patterns of the surface charge. At the same time, the elution time of the second peak in the XIC of the non-phosphorylated species (peak F in **Figure 3**) is anomalous, as the same retention is exhibited by the di-phosphorylated

species (peak D) carrying two additional negative charges. This apparent contradiction is resolved by examining the mass spectra averaged across the elution windows corresponding to peaks A and F: an overlay of ion peaks at *m/z* 3824 provides unequivocal evidence that these two peaks do in fact represent different ionic species (see the bottom left panel in **Figure 3**) whose masses are too close to each other to avoid interference in XIC (in contrast, the profiles of ionic signals at *m/z* 3380 averaged across the elution windows corresponding to peaks B and C in **Figure 3** overlap completely, confirming that they represent truly isobaric species, *i.e*. two isomeric forms of the mono-phosphorylated species).

Although one might be tempted to explain the appearance of the "extra" peak in the XIC of the non-phosphorylated species in **Figure 3** as a result of deamidation (which would increase the total negative charge on the protein, extending its retention on the anion exchange column), this appears unlikely. First, deamidation increases the protein mass by 0.98 Da, while the ionic mass of species F decreases by 1.9 Da compared to species A (see the bottom left panel in **Figure 3**). Second, the elution time of peak F coincides with that of the di-phosphorylated species (labeled D in **Figure 3**), which has two, rather than one, extra negative charges compared to the species A. A more likely explanation for the presence of peak D in the chromatogram invokes the presence of a different glycoform having a surface charge density pattern similar or indeed identical to that of species D. For example, the mass of the di-phosphorylated form of the glycoform $Hex_8GlcNAc_8NeuAc_0$ (1-2-0-0-8-8-0) should be 2 Da below that of species A (consistent with the observed mass difference of 1.9 Da between species A and F in **Figure 3**). Thus, on-line IXC/MS analysis of OVA sample allows all four different phosphorylation forms of a single protein glycoform to be identified, a task that cannot be accomplished by MS alone.[7] Detailed analysis of the entire complement of different OVA proteoforms (***Table S2*** in ***Supplementary Information***) confirms that nearly all OVA glycoforms are represented by several different phosphorylation states.

Unlike phosphorylation, acetylation of the N-terminus is a PTM type that affects OVA on a nearly-uniform basis.[26] It is therefore not surprising that the vast majority of OVA

proteoforms detected in this work (129 out of a total of 138) appear to be acetylated (see ***Table S2*** in ***Supplementary Information*** for more detail). The nine detected non-acetylated forms of the protein are represented by low-abundance ionic species, with intensities being nearly two orders of magnitude below those of their acetylated counterparts. An example is shown in **Figure 4**, where the de-acetylated from of the glycoform $Hex_6GlcNAc_2NeuAc_0$ (0-1-0-0-6-2-0) elutes prior to its acetylated counterpart. This elution order is not surprising, since this PTM neutralizes a basic site on the protein surface, increasing its net negative charge.

Although OVA is not glycosylated as extensively as OVM, glycosylation is undoubtedly the single largest source of its structural microheterogeneity.[7, 21] While $Hex_nGlcNAc_mNeuAc_k$ (where n, m and k are confined to the following ranges: $3 \le n \le 10$, $2 \le m \le 1$, and $0 \le k \le 1$) is generally considered a typical glycan chain template for OVA,[28] IXC/MS allows us to detect glycoproteins with carbohydrate chains ranging from as few as six monosaccharide units ($Hex_4GlcNAc_2NeuAc_0$) to as many as twenty (e.g., $Hex_9GlcNAc_{11}NeuAc_0$), see ***Table S2*** in ***Supplementary Information*** for more detail. Not more than a single sialic acid residue is incorporated into a glycan chain. Intriguingly, only relatively short carbohydrate chains (ranging from 7 to 12 monosaccharide units) contain sialic acid residues. Although the specific reason(s) for such selectivity remains unclear, we note that this observation is consistent with earlier reports.[37] Another intriguing observation is the presence of the carbohydrate-free (a-glycosylated) forms of the protein in the OVA sample (**Figure 5**), which have not been reported for the wild-type OVA previously. Since the sample handling was minimal in our work, and no hydrolytic enzymes or chemicals were used, we conclude that the carbohydrate-free form of OVA represents a-glycosylated (rather than de-glycosylated) OVA molecules, which were present in the initial sample at low abundance. Due to their low abundance, these species had escaped detection previously, and it is the on-line IXC/MS that allowed them to be detected and identified within the protein sample.

Not surprisingly, the presence of an acidic NeuAc unit within the carbohydrate chain results in a significant increase of the retention time; however, a nearly identical increase of the

retention time is observed as a result of the absence of the carbohydrate chain (**Figure 5**). Furthermore, careful analysis of the retention time of different glycoforms indicates that even small variations of the number of neutral saccharide units within the glycan chain result in small but consistent changes in the retention characteristics of OVA proteoforms. Thus, decreasing the total number of either Hex or GlcNAc residues within the carbohydrate chain by a single saccharide unit results in a slightly enhanced retention (**Figure 6**). This behavior would be expected in the HILIC mode of separation,[38] but is surprising to observe in ion exchange. Most likely, the correlation between the size of the carbohydrate chain and the retention time is not due to the marginal basicity of the neutral saccharide residues, but rather reflects the charge shielding properties of the glycan. Indeed, several negative charges (acidic side chains) on the OVA surface are located near the glycosylation site (Asn-292), and are likely to be at least partially shielded from the cationic resin by the solvent-exposed carbohydrate chain (see ***Figure S1*** in ***Supplementary Information***). Reduction of this surface charge shielding in glycoforms with shorter carbohydrate chains (or indeed complete elimination of this shielding in the glycan-free OVA) would result in enhanced interaction of the protein with the anion exchange resin and, as a result, delayed elution.

The most prominent non-enzymatic PTM revealed by on-line IXC/MS is oxidation (see ***Table S2*** in ***Supplementary Information*** for more detail). As expected, oxidation results in an increase of the retention time: for example, the three OVA isoforms whose elution profiles are presented in **Figure 6** are retained on the column for an additional 4 minutes compared to their non-oxidized counterparts (which comprise the most abundant chromatographic peak). This enhanced retention likely reflects the increase of the acidic character of proteins caused by oxidation without introducing a formal negative charge.[39, 40] One intriguing conclusion from the analysis of the entire complement of all oxidized OVA isoforms relates to the fact that this PTM is detected only among the proteoforms carrying two phosphate groups. The hypothesis that at least some PTMs within a single protein may be correlated has been attracting attention within the functional proteomics field in recent years.[41, 42] However, it must be emphasized that

one of the two PTMs showing an apparent correlation in OVA is non-enzymatic (oxidation), and no correlations involving irreversible non-enzymatic PTMs are known at present.[43] Far from having any functional importance, the observed correlation between OVA oxidation and its phosphorylation most likely reflects the increased susceptibility of the protein to oxidation once it is fully phosphorylated, the specific chemical causes of which are yet to be elucidated.

One of the challenges that have been encountered during the analysis of OVA proteoforms detected by IXC/MS is the existence of some species with close/identical masses. We have already mentioned the appearance of an interfering ionic species in the XIC for the OVA glycoform $Hex_9GlcNAc_8NeuAc_0$ lacking phosphorylation (*m/z* 3824), where the late eluting species (peak F in **Figure 3**) was identified as (1-2-0-0-8-8-0), a di-phosphorylated form of the glycoform $Hex_8GlcNAc_8NeuAc_0$. In that particular case identification of the interfering species was aided by analyzing the elution patterns of isoforms differing from each other by the extent of phosphorylation; a slight mass difference between the two ions at *m/z* 3823 was also apparent (as discussed earlier). Furthermore, XIC plots generated for *m/z* values corresponding to the putative forms (1-1-0-0-8-8-0) and (1-0-0-0-8-8-0) (see ***Figure S2*** in ***Supplementary Information***) reveal both elution patterns and intensity ratios similar to those exhibited by (1-1-0-0-9-8-0) and (1-0-0-0-9-8-0) proteoforms (as shown in **Figure 3**). Similar analyses can be carried out in many other cases enabling annotation of the entire chromatogram (**Figure 7**), although data interpretation based solely on intact mass measurements should always be treated with caution.

Quantitation of different isoforms is another serious issue that remains to be addressed. Although rough estimates of the relative abundance of different isoforms can be obtained by comparing ionic signal intensities, the latter are influenced by a range of other factors besides fractional concentration of the corresponding species in solution. For example, comparing the relative abundance of the ionic signals for the (1-2-0-0-9-8-0), (1-1-0-0-9-8-0) and (1-0-0-0-9-8-0) proteoforms gives an estimate of bis-phosphorylated vs. mono-phosphorylated vs. non-phosphorylated species as near 15:11:1 (**Figure 3**). Similar ratios can be obtained for the

majority of other OVA glycoforms. However, the consensus ratio is 8:2:1,[3] suggesting that quantitation based on the intensity of the ionic signal in IXC/MS results in an underestimation of the relative abundance of the fully phosphorylated OVA molecules. This should not be surprising, since each phosphorylation introduces an extra negative charge on the protein surface, which is expected to diminish the number of electrospray-generated polycationic species representing this particular isoform.[44-46] Another parameter affecting the response factor is the elution time of the species in question: using salt gradient as a means of facilitating the elution process means that the ions representing later-eluting species would be generated from solutions with higher electrolyte concentrations. The latter is known to affect both the charge state distributions and the intensity of ionic ensembles in ESI MS,[47-50] thereby further complicating the proteoform quantitation based on the strength of their ionic signal. Despite this drawback, IXC/MS should be ideally suited for situations when a comparison needs to be made between two different samples. In such situations, a comparison of the relative abundance of the ionic signal for the same isoform in two different samples enables meaningful inter-sample quantitation.

3.2 Relationship between structural heterogeneity and IgG/IgE binding of OVA

Localization of PTMs to specific regions of the protein chromatogram (Figure 7) provides an opportunity to establish the correlations between the immunoglobulin-binding properties of the protein and specific structural features that commonly occur in intact (unprocessed) OVA. In order to explore the relationship between structural heterogeneity and IgG/IgE binding of OVA, several OVA fractions in IXC were collected (representing twelve elution windows as shown in Figure 7). The IgG and IgE binding properties of these OVA fractions were then compared based on their IC_{50} values. The SEC-purified OVA was the substrate while the OVA fractions were the inhibitors. The IC_{50} value is the inhibitor concentration that causes a 50% inhibition of the antibody binding capacity: the higher the IC_{50} value, the lower the binding capacity. As shown in Figure 8, the IC_{50} values of IgG were correlated well with those of IgE. The IC_{50} values of P1-P3 were much higher than that of SEC-purified OVA, indicating that their IgG

and IgE binding capacities were lower. This effect can be attributed to the presence of OVM in these fractions, which had no specific binding to anti-OVA-sera. Nevertheless, the rabbit antisera were specific to OVA while HEA patient antisera were specific to hen egg, which contains OVM. When OVA fractions containing OVM impurities were added as inhibitors, both OVA and OVM would bind to the HEA patient antisera and lead to a decrease in IC_{50} value. Therefore, the IgG IC_{50} value is overall higher than the IgE IC_{50} value of P1-P3.

Moreover, the IC_{50} values of bis-phosphorylated isoforms were higher than that of the mono-phosphorylated ones, implying that phosphorylation weakened the IgG and IgE binding of OVA. The IgG and IgE binding capacities of OVA were determined using IgG and IgE epitopes, including sequential and conformational epitopes. Numerous studies have been carried out to identify the IgG and IgE epitopes of OVA, which have shown that the IgG and IgE epitopes are widely spread along the whole sequence of OVA[1]. PTMs, such as phosphorylation[6], acetylation[51], oxidation and succinimide formation[39], could modify or mask both the sequential epitopes of IgG and IgE by covalent modification. The different elution time of OVA in IXC also suggests that PTMs could induce their conformational changes, which destroy some conformational epitopes of IgG and IgE. Finally, OVA isoforms with PTMs are more difficult to be recognized by IgG or IgE due to sequence modification and consequent conformational changes caused by PTMs. This explains why the IC_{50} values of P4 and P9 were about 20% lower than those of P5 and P12. Moreover, P9 had higher IgG and IgE IC_{50} values than P11, suggesting that the different phosphorylation sites could result in different IgG and IgE binding capacities through sequence modification and conformational changes. However, P9 had about 25% higher values than P10, indicating that the OVA proteoforms with sialic acid-containing glycans had higher IgG and IgE binding capacities. Previous studies have also reported that sialic acid-containing glycans increased the IgG/IgE binding capacity.[37] Therefore, the reason that P7 had lower IgG and IgE IC_{50} values than P5 may have been because of differences in their phosphorylation sites and sialic acid-containing glycans. Furthermore, the IC_{50} values of mono-phosphorylated OVA were lower than that of di-phosphorylated ones,

implying that OVA proteoforms with fewer modifications have higher IgG/IgE binding capacities. The P9 fraction had over 20% lower IgG and IgE IC_{50} values than P8, which could be attributed to succinimide formation and the presence of a long carbohydrate chain, which promoted folding and increased the stability of the glycoprotein[52]. As a result, the recognition of IgG or IgE was hindered, leading to a lower IgG/IgE binding capacity.

4. Conclusion

In summary, on-line IXC-MS with salt gradient elution was shown to be a powerful tool for the characterization of the structural heterogeneity of ovalbumin caused by post-transcription modifications. Over a hundred and thirty different ovalbumin proteoforms were identified based on their elution times and/or masses. Besides, eighty-four different glycoforms of ovomucoid were detected, which was a low-level protein impurity in the OVA sample that completely escaped detection by MS alone. The relationship between the structural heterogeneity and IgG/IgE binding of OVA was explored. This analysis helped to identify structural modifications of OVA that led to higher or lower allergenicity. The IXC/MS method is relatively rapid, involves only one step (a single LC/MS run), and does not require any chemical/enzymatic (pre)treatment of the protein sample, thereby making it ideally suited for situations where a rapid assessment of protein quality is required. Improved knowledge of the relationship between IgG/IgE binding capacity and OVA heterogeneity caused by post-translational modifications may lead to the development of new biotechnology or food processing strategies for reducing the allergenicity of egg products. For instance, chemical reactions such as oxidation and phosphorylation may occur during the processing or storage of food proteins, and so it may be possible to decrease the allergenicity of OVA by controlling these reactions. This information may also be important for the emerging field of cellular agriculture, where protein ingredients are being created using microbial fermentation methods.

Conflicts of interest

There are no conflicts to declare.

Acknowledgments

This work was supported by the National Natural Science Foundation of China (No. 32001644) and the National Science Foundation (CHE-1709552). W.Y. also acknowledges support from Gthe China Scholarship Council. The authors are grateful to Drs. Cedric E. Bobst, Shengsheng Xu and Yunlong Zhao for their help with setting up IXC/MS experiments.

References

1. W.-H. Yang, Z.-C. Tu, H. Wang, X. Li and M. Tian, *J. Sci. Food Agric.*, 2017, **97**, 2714-2720.
2. N. J. Osborne, J. J. Koplin, P. E. Martin, L. C. Gurrin, A. J. Lowe, M. C. Matheson, A.-L. Ponsonby, M. Wake, M. L. K. Tang, S. C. Dharmage and K. J. Allen, *J. Allergy Clin. Immunol.*, 2011, **127**, 668-676.e662.
3. J. A. Huntington and P. E. Stein, *J. Chromatogr. B Biomed. Sci. Appl.*, 2001, **756**, 189-198.
4. R. D. J. Huby, R. J. Dearman and I. Kimber, *Toxicol. Sci.*, 2000, **55**, 235-246.
5. F. Altmann, *Toxicol. Sci.*, 2007, **142**, 99-115.
6. B. Cases, C. García-Ara, M. T. Boyano, M. Pérez-Gordo, M. Pedrosa, F. Vivanco, S. Quirce and C. Pastor-Vargas, *J. Investig. Allergol. Clin. Immunol.*, 2011, **21**, 398-400.
7. Y. Yang, A. Barendregt, J. P. Kamerling and A. J. Heck, *Anal. Chem.*, 2013, **85**, 12037-12045.
8. T. Kristl and H. Stutz, *J. Sep. Sci.*, 2015, **38**, 148-156.
9. S. Wang, C. E. Bobst and I. A. Kaltashov, *Anal. Chem.*, 2011, **83**, 7227-7232.
10. P. Mallick and B. Kuster, *Nat. Biotech.*, 2010, **28**, 695-709.
11. S. Fekete, A. Beck, J.-L. Veuthey and D. Guillarme, *J. Pharm. Biomed. Anal.*, 2013, **113**, 43-55.
12. K. Muneeruddin, M. Nazzaro and I. A. Kaltashov, *Anal. Chem.*, 2015, **87**, 10138-10145.
13. I. A. Kaltashov and R. R. Abzalimov, *J. Am. Soc. Mass Spectrom.*, 2008, **19**, 1239-1246.
14. I. A. Kaltashov and A. Mohimen, *Anal. Chem.*, 2005, **77**, 5370-5379.
15. L. Testa, S. Brocca and R. Grandori, *Anal. Chem.*, 2011, **83**, 6459-6463.
16. K. Muneeruddin, C. E. Bobst, R. Frenkel, D. Houde, I. Turyan, Z. Sosic and I. A. Kaltashov, *Analyst*, 2017, **142**, 336-344.
17. Y. Leblanc, C. Ramon, N. Bihoreau and G. Chevreux, *J. Chromatogr. B Analyt. Technol. Biomed. Life Sci.*, 2017, **1048**, 130-139.
18. F. Fussl, K. Cook, K. Scheffler, A. Farrell, S. Mittermayr and J. Bones, *Anal. Chem.*, 2018,

90, 4669-4676.

19. F. Fussl, A. Trappe, S. Carillo, C. Jakes and J. Bones, *Anal. Chem.*, 2020, DOI: 10.1021/acs.analchem.0c00185.
20. S. Xu and I. A. Kaltashov, *Mol. Pharm.*, 2017, **14**, 2843–2851.
21. F. Füssl, A. Criscuolo, K. Cook, K. Scheffler and J. Bones, *J. Proteome Res.*, 2019, **18**, 3689-3702.
22. W. Yang, Z. Tu, H. Wang, L. Zhang, I. A. Kaltashov, Y. Zhao, C. Niu, H. Yao and W. Ye, *Food Funct.*, 2018, **9**, 417-425.
23. W. Yang, Z. Tu, H. Wang, L. Zhang, S. Xu, C. Niu, H. Yao and I. A. Kaltashov, *J. Agr. Food Chem.*, 2017, **65**, 8018-8027.
24. I. Roy, M. V. S. Rao and M. N. Gupta, *Appl. Biochem. Biotechnol.*, 2003, **111**, 55-63.
25. I. A. Kaltashov, C. E. Bobst and R. R. Abzalimov, *Protein Sci.*, 2013, **22**, 530-544.
26. A. D. Nisbet, R. H. Saundry, A. J. Moir, L. A. Fothergill and J. E. Fothergill, *Eur. J. Biochem.*, 1981, **115**, 335-345.
27. K. Mann and M. Mann, *Proteome Sci.*, 2011, **9**, 7.
28. D. J. Harvey, D. R. Wing, B. Küster and I. B. H. Wilson, *J. A. Soc. Mass Spectrom.*, 2000, **11**, 564-571.
29. M. Thaysen-Andersen, S. Mysling and P. Højrup, *Anal. Chem.*, 2009, **81**, 3933-3943.
30. Q. P. Lei, X. Cui, D. M. Kurtz, Jr., I. J. Amster, I. V. Chernushevich and K. G. Standing, *Anal. Chem.*, 1998, **70**, 1838-1846.
31. W. P. Griffith and I. A. Kaltashov, *Biochemistry*, 2003, **42**, 10024-10033.
32. P. Lossl, J. Snijder and A. J. Heck, *J. Am. Soc. Mass Spectrom.*, 2014, **25**, 906-917.
33. J. Lu, M. J. Trnka, S. H. Roh, P. J. Robinson, C. Shiau, D. G. Fujimori, W. Chiu, A. L. Burlingame and S. Guan, *J. Am. Soc. Mass Spectrom.*, 2015, **26**, 2141-2151.
34. J. W. Pawlowski, N. Kellicker, C. E. Bobst and I. A. Kaltashov, *Analyst*, 2016, **141**, 853-861.
35. H. Li, J. J. Wolff, S. L. Van Orden and J. A. Loo, *Anal. Chem.*, 2014, **86**, 317-320.
36. L. He, L. C. Anderson, D. R. Barnidge, D. L. Murray, C. L. Hendrickson and A. G.

Marshall, *J. Am. Soc. Mass Spectrom.*, 2017, **28**, 827-838.

37. K. Yamashita, Y. Tachibana, A. Hitoi and A. Kobata, *Carbohydr. Res.*, 1984, **130**, 271-288.
38. E. Domínguez-Vega, S. Tengattini, C. Peintner, J. van Angeren, C. Temporini, R. Haselberg, G. Massolini and G. W. Somsen, *Talanta*, 2018, **184**, 375-381.
39. Y. Leblanc, C. Ramon, N. Bihoreau and G. Chevreux, *J. Chromatogr. B*, 2017, **1048**, 130-139.
40. G. Ponniah, A. Kita, C. Nowak, A. Neill, Y. Kori, S. Rajendran and H. Liu, *Anal. Chem.*, 2015, **87**, 9084-9092.
41. P. Beltrao, P. Bork, N. J. Krogan and V. van Noort, *Mol. Syst. Biol.*, 2013, **9**, 714.
42. M. Audagnotto and M. Dal Peraro, *Comput. Struct. Biotechnol. J.*, 2017, **15**, 307-319.
43. R. Harmel and D. Fiedler, *Nat. Chem. Biol.*, 2018, **14**, 244-252.
44. N. B. Cech and C. G. Enke, *Mass Spectrom. Rev.*, 2001, **20**, 362-387.
45. M. Samalikova and R. Grandori, *J. Mass Spectrom.*, 2003, **38**, 941-947.
46. J. Li, C. Santambrogio, S. Brocca, G. Rossetti, P. Carloni and R. Grandori, *Mass Spectrom. Rev.*, 2016, **35**, 111-122.
47. D. R. Gumerov, A. Dobo and I. A. Kaltashov, *Eur. J. Mass Spectrom.*, 2002, **8**, 123-129.
48. A. K. Frimpong, R. R. Abzalimov, S. J. Eyles and I. A. Kaltashov, *Anal. Chem.*, 2007, **79**, 4154-4161.
49. J. B. Hedges, S. Vahidi, X. Yue and L. Konermann, *Anal. Chem.*, 2013, **85**, 6469-6476.
50. L. Konermann, H. Metwally, Q. Duez and I. Peters, *Analyst*, 2019, **144**, 6157-6171.
51. R. Ree, S. Varland and T. Arnesen, *Exp. Mol. Med.*, 2018, **50**, 1-13.
52. V. Ortega, J. A. Stone, E. M. Contreras, R. M. Iorio and H. C. Aguilar, *Glycobiology*, 2018, **29**, 2-21.

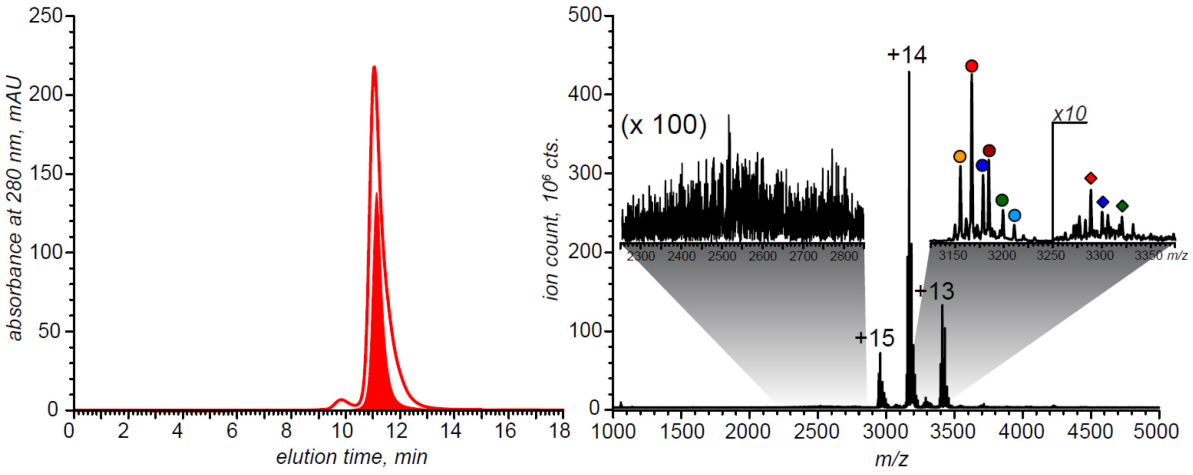

GSIGAASMEF CFDVFKELKV HHANENIFYC PIAIMSALAM VYLGAKDSTR TQINKVVRFD[60]

KLPGFGDSIE AQCGTSVNVH SSLRDILNQI TKPNDVYSFS LASRLYAEER YPILPEYLQC[120]

VKELYRGGLE PINFQTAADQ ARELINSWVE SQTNGIIRNV LQPSSVDSQT AMVLVNAIVF[180]

KGLWEKAFKD EDTQAMPFRV TEQESKPVQM MYQIGLFRVA SMASEKMKIL ELPFASGTMS[240]

MLVLLPDEVS GLEQLESIIN FEKLTEWTSS NVMEERKIKV YLPRMKMEEK YNLTSVLMAM[300]

GITDVFSSSA NLSGISSAES LKISQAVHAA HAEINEAGRE VVGSAEAGVD AASVSEEFRA[360]

DHPFLFCIKH IATNAVLFFG RCVSP[385]

Figure 1. Top: SEC purification of OVA (the color-filled curve shows the SEC re-run of the collected fraction) and the native ESI mass spectrum of the collected SEC fraction. Colored circles and diamonds refer to the main detected OVA species. Bottom: the amino acid sequence of OVA (Swiss-Prot P01012) with the known PTMs sites highlighted. G1 is N-terminal acetylation sites. S68 and S344 is phosphorylation sites. N292 is glycosylation site.

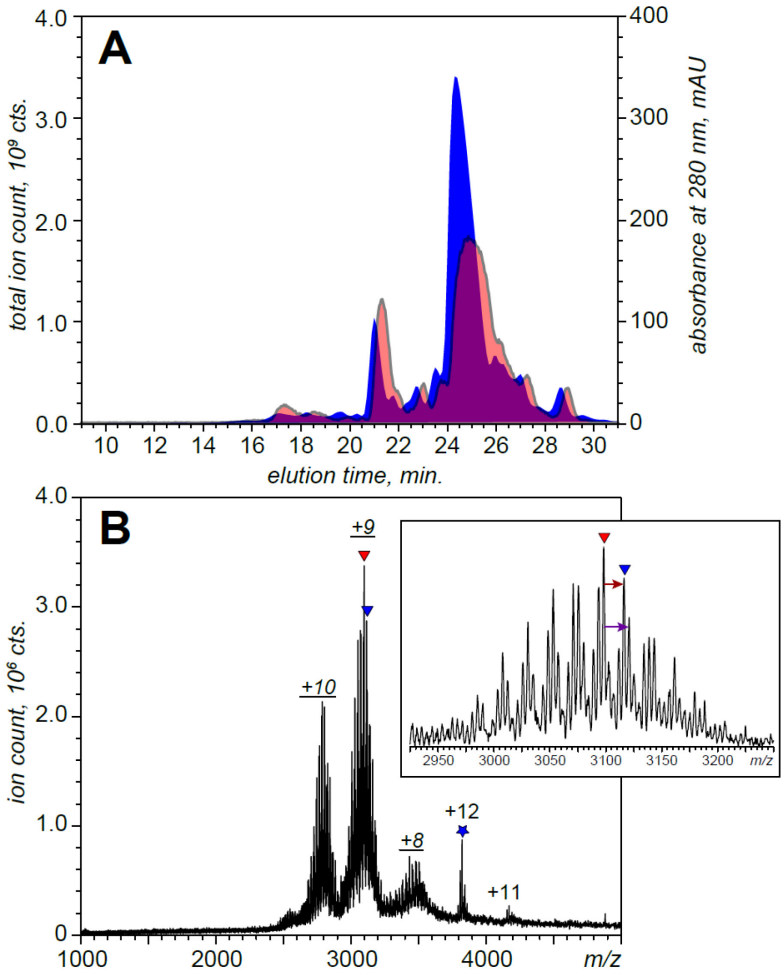

552

553 **Figure 2.** Ion exchange chromatograms with UV absorption detection shown in blue and total
554 ion chromatogram generated by on-line native ESI MS detection shown in red (A) and a
555 representative on-line mass spectrum averaged across the 17-18 min elution window (B). The
556 ion peaks labeled with red and blue triangles represent the $Hex_{18}GlcNAc_{24}NeuAc_0$ and
557 $Hex_{19}GlcNAc_{24}NeuAc_0$ glycoforms of OVM, respectively. The inset shows a zoomed view of
558 the *m/z* region of the mass spectrum containing signal of OVM ions at +9 charge state (the
559 brown and purple arrows indicate m/z shifts due to the addition of a hexose residue and a
560 GlcNAc residue, respectively). The ion peak labeled with a star represents the P1-4(1-0-0-0-9-
561 8-0) species of OVA.

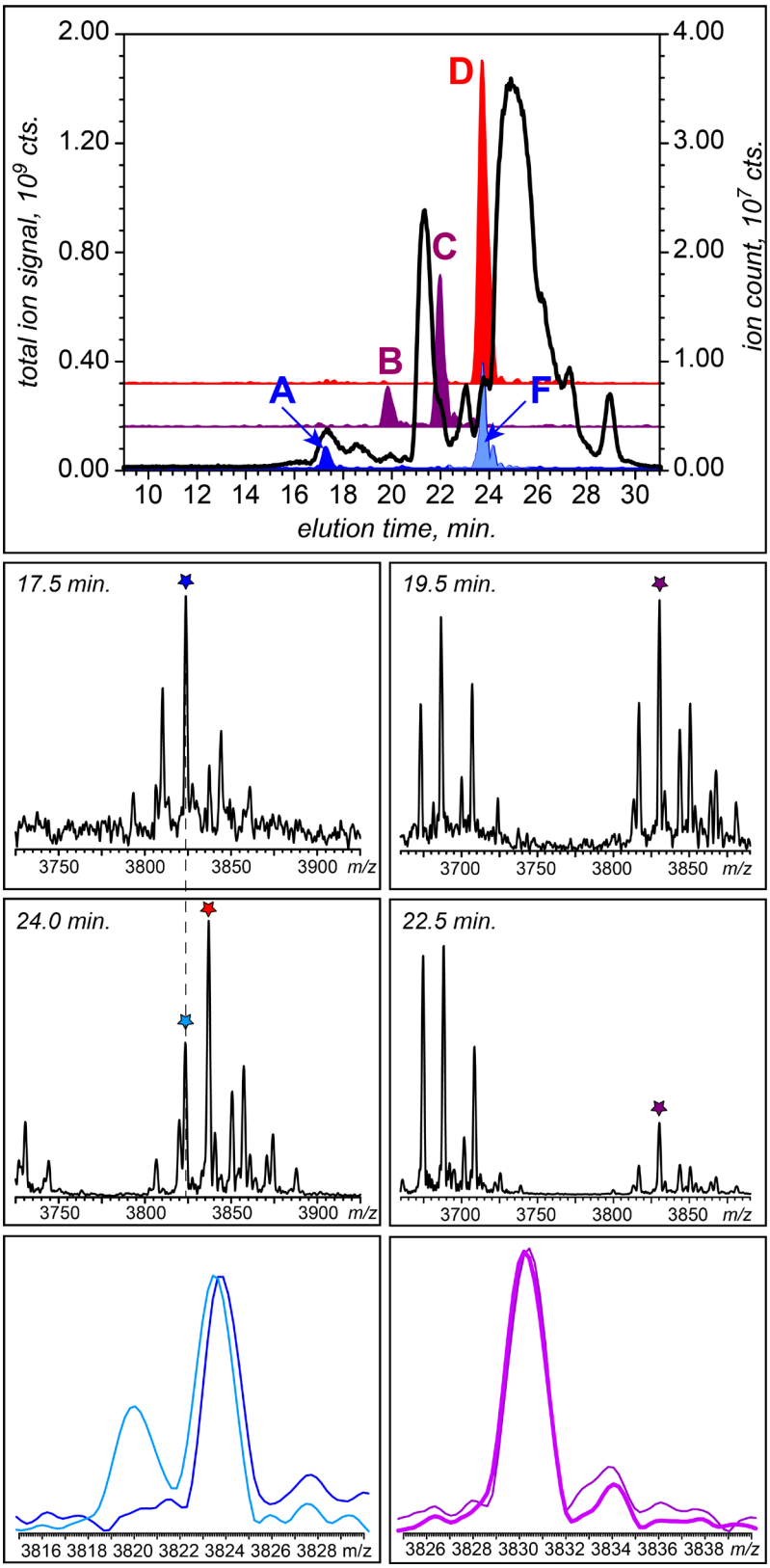

562

563 **Figure 3**. Influence of phosphorylation on OVA elution in anion-exchange chromatography.

564 Top: extracted ion chromatograms for OVA glycoform $Hex_9GlcNAc_8NeuAc_0$ exhibiting

565 different levels of phosphorylation (blue: non-phosphorylated; purple: mon-phosphorylated;
566 and red: bis-phosphorylated) and no other non-enzymatic PTMs (total ion chromatogram is
567 also shown for reference). Middle: ionic signals used to construct the XICs in the top panel
568 (mass spectra are averaged across the elution windows as indicated on each panel), as indicated
569 with color-coded stars. Bottom: overlays of signal profiles giving rise to a pair of peaks in the
570 XIC of the non-phosphorylated species (blue and pale blue) and a pair of peaks in the XIC of
571 the mono-phosphorylated species (two shades of purple).

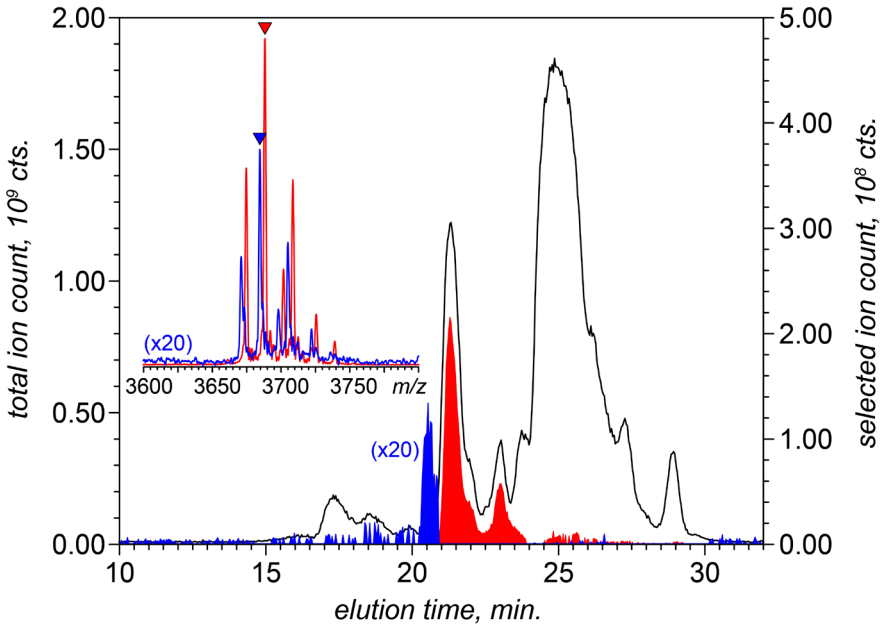

572

573 **Figure 4**. Effect of N-terminal acetylation of OVA on its elution in anion-exchange
574 chromatography: XIC profiles of (0-1-0-0-6-2-0) and (1-1-0-0-6-2-0), shown in blue and red,
575 respectively. The inset shows the zoomed views of mass spectra averaged across the 20-21 min
576 and 21-22 min elution windows (relevant ionic peaks are labeled with the appropriately color-
577 coded triangles).

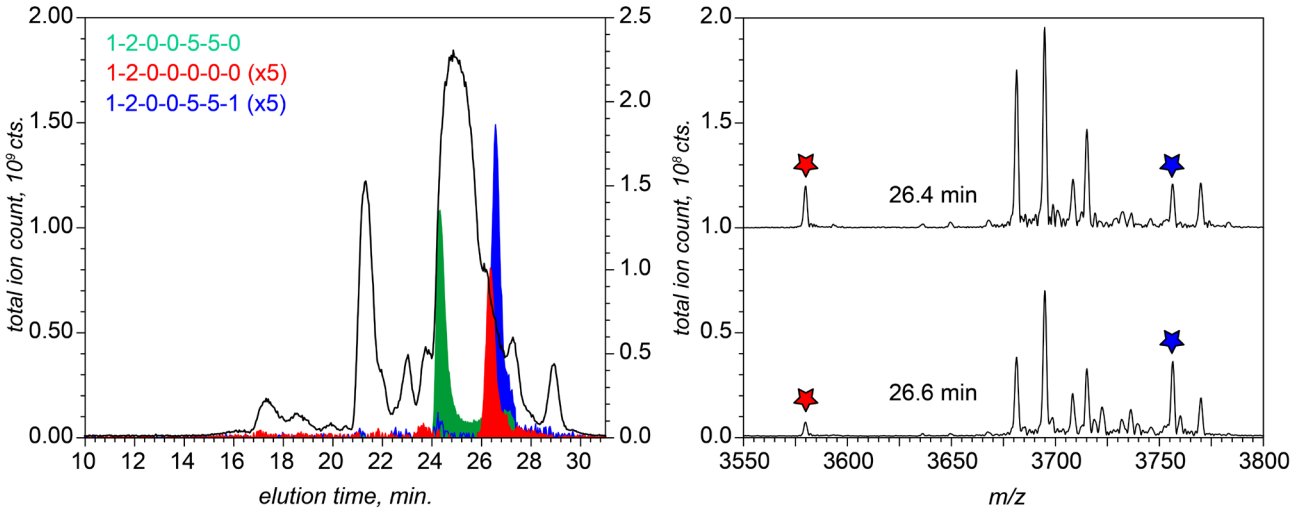

578

579 **Figure 5**. Influence of OVA glycosylation on its elution in anion-exchange chromatography:
580 XIC profiles of the a-glycosylated form (1-2-0-0-0-0-0) and two representative glycoforms (1-
581 2-0-0-5-5-0) and (1-2-0-0-5-5-1) carrying the same number of phosphate groups (colored in
582 blue, green and red, respectively). The ion peaks representing the two glycoforms are labeled
583 with stars in the on-line mass spectra that were collected 20 sec. apart from each other (shown
584 in the pane on the right).

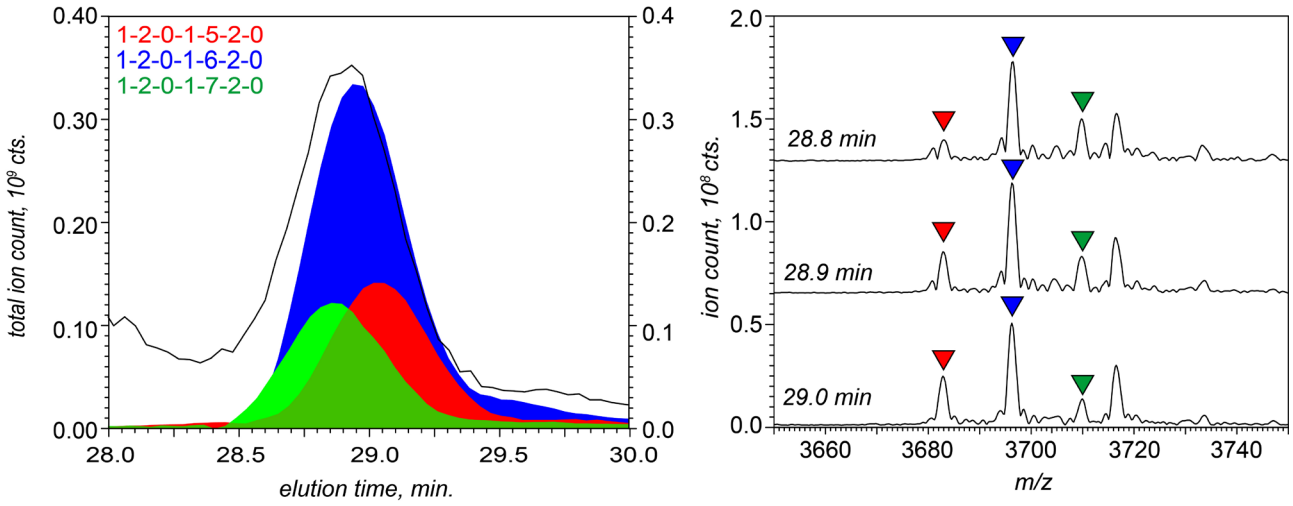

586 **Figure 6**. Influence of incremental variation in the glycan chain composition on OVA elution
587 in anion-exchange chromatography: XIC profiles of (1-2-0-1-5-2-0), (1-2-0-1-6-2-0) and (1-2-
588 0-1-7-2-0) isoforms eluting over a narrow window 28.5-29.5 min (red, blue, and green,
589 respectively). The ion peaks representing these glycoforms are labeled with appropriately
590 color-coded triangles in representative on-line mass spectra that were collected within the same
591 elution window (shown in the pane on the right).

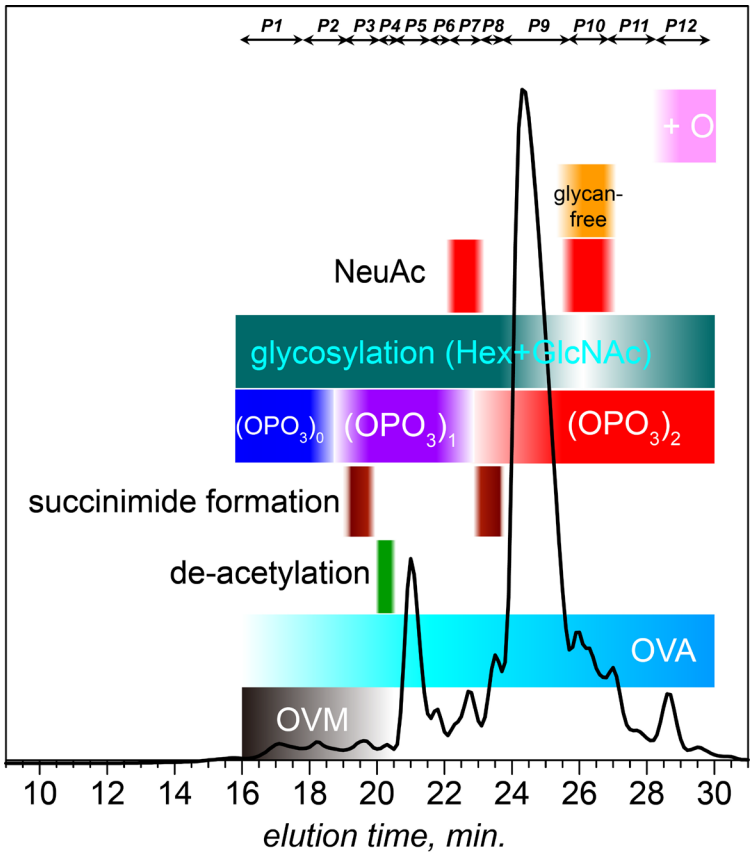

592

593 **Figure 7**. Annotated IXC chromatogram of the SEC-purified OVA sample. $(OPO_3)_0$, $(OPO_3)_1$
594 and $(OPO_3)_2$ refers non-phosphorylated, mono-phosphorylated and bis-phosphorylated OVA,
595 respectively. +O represents the OVA species with oxidation. Glycoylation (Hex+GlcNAc)
596 refers the OVA proteoforms with glycan on N292 while NeuAc refers to those have glycan
597 with N-acetylneuraminic acid / sialic acid.

598

599 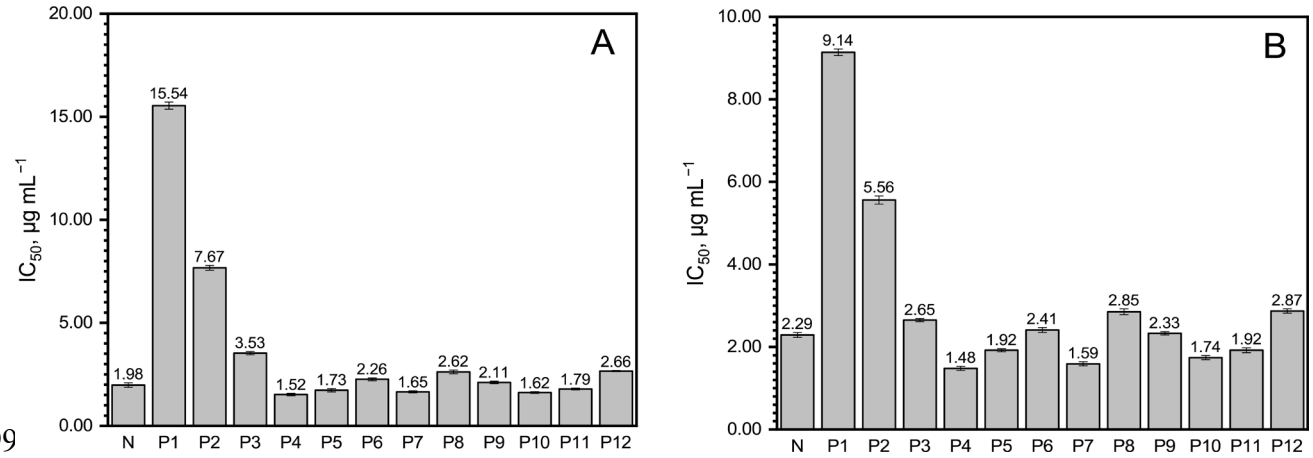

600 **Figure 8**. IgG binding (A) and IgE binding (B) of OVA structural heterogeneity caused by
601 different PTMs. N presents the SEC-purified native OVA. P1-P12 refers the collected peaks of
602 SEC-purified native OVA according to the UV absorbance.

603 **Graphical abstracts**

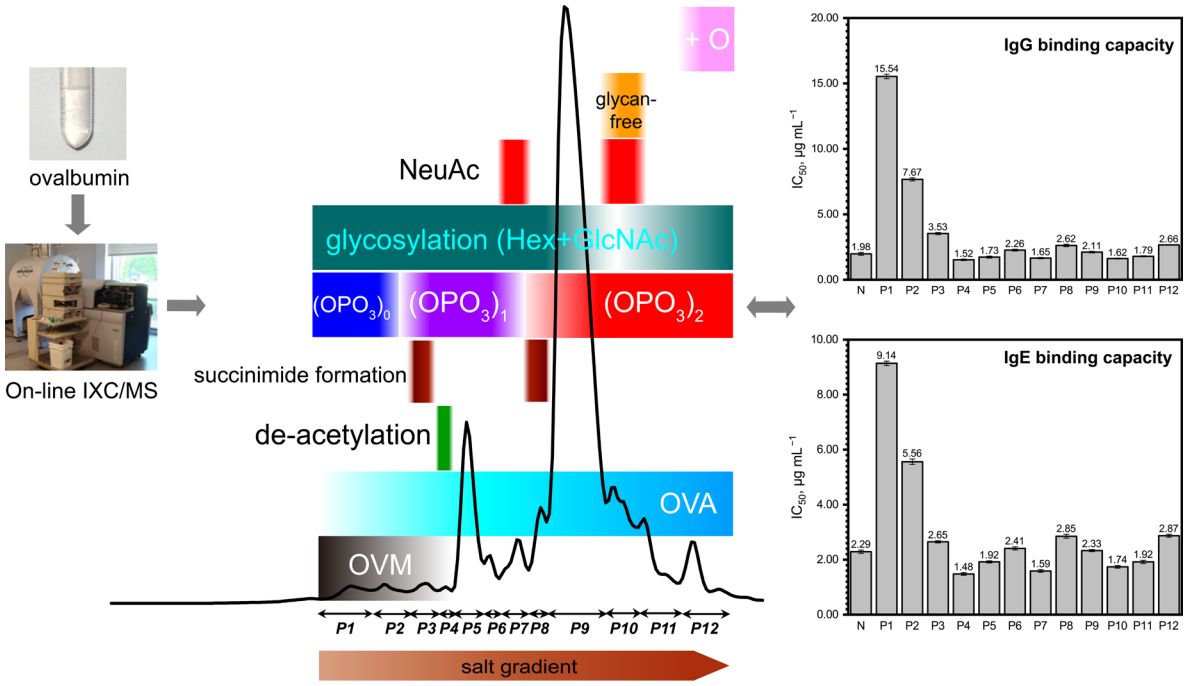

604